Marangoni spreading due to a localized alcohol supply on a thin water film

José Federico Hernández-Sánchez, Antonin Eddi, and J. H. Snoeijer

Citation: Physics of Fluids (1994-present) **27**, 032003 (2015); doi: 10.1063/1.4915283
View online: http://dx.doi.org/10.1063/1.4915283
View Table of Contents: http://scitation.aip.org/content/aip/journal/pof2/27/3?ver=pdfcov
Published by the AIP Publishing

PHYSICS OF FLUIDS **27**, 032003 (2015)

Marangoni spreading due to a localized alcohol supply on a thin water film

José Federico Hernández-Sánchez,[1] Antonin Eddi,[1] and J. H. Snoeijer[1,2]
[1]*Physics of Fluids Group, Faculty of Science and Technology, J.M. Burgers Center for Fluid Dynamics, University of Twente, P.O. Box 217, 7500 AE Enschede, The Netherlands*
[2]*Department of Applied Physics, Eindhoven University of Technology, P.O. Box 513, 5600MB Eindhoven, The Netherlands*

(Received 1 September 2014; accepted 17 February 2015; published online 24 March 2015)

Bringing two miscible fluids into contact naturally generates strong gradients in surface tension. Here, we investigate such a Marangoni-driven flow by continuously supplying isopropyl alcohol (IPA) on a film of water, using micron-sized droplets of IPA-water mixtures. These droplets create a localized depression in surface tension that leads to the opening of a circular, thin region in the water film. At the edge of the thin region, there is a growing rim that collects the water of the film, reminiscent of Marangoni spreading due to locally deposited surfactants. In contrast to the surfactant case, the driving by IPA-water drops gives rise to a dynamics of the thin zone that is independent of the initial layer thickness. The radius grows as $r \sim t^{1/2}$, which can be explained from a balance between Marangoni and viscous stresses. We derive a scaling law that accurately predicts the influence of the IPA flux as well as the thickness of the thin film at the interior of the spreading front. © *2015 AIP Publishing LLC.* [http://dx.doi.org/10.1063/1.4915283]

I. INTRODUCTION

Liquids of spatially inhomogeneous composition will exhibit surface tension gradients, which induces nontrivial flow. A famous example of such a Marangoni flow are the tears of wine,[1] where selective evaporation of alcohol is the origin of complicated droplet patterns. A similar effect is exploited in the industrial technique called Marangoni drying, where the Marangoni forces, due to vapor adsorption, induce local gradients in composition.[2,3] This is an effective technique for achieving very clean surfaces, of particular importance in semiconductor industry. Though substantial theoretical understanding was achieved,[4,5] some unexpected coalescence phenomena were recently reported. When two miscible droplets of different chemical composition are brought into contact, the Marangoni forces can delay or prevent actual coalescence.[6–10] The coalescence is frustrated by the very localized gradient of surface tension in the "neck" region. In contrast to the growth of the neck as in normal coalescence,[11–14] the drops exhibit a translational motion where the drop of larger surface tension pulls the other drop over the substrate.[7,9]

The purpose of the present work is to investigate the Marangoni flow by localized deposition of alcohol on a thin water film. These droplets create a localized depression in surface tension that leads to the opening of a circular, thin region in the water film (see Fig. 1). The observed structure reminiscent of a hydraulic jump (see, for example, Refs. 15 and 16). Nevertheless, the physical driving mechanism and the nature of the flow are different. For a hydraulic jump, the structure reaches a steady state, and the location of the jump is set by inertial effects, when the Froude number is of order unity.[17] In our case, the viscous dominated flow is driven by Marangoni effects and the hole expands continuously with time.

This is a geometry that has been extensively studied for surfactants, creating a similar surface tension gradient and radially outward flow.[18–31] This class of experiments is called "surfactant spreading," that typically exhibits power-law dynamics of the spreading radius versus time, i.e., $r \sim t^{\alpha}$. Many different cases have been identified, leading to a variety of exponents: surfactants can be soluble or insoluble, can be supplied at different rates and in different geometries, while

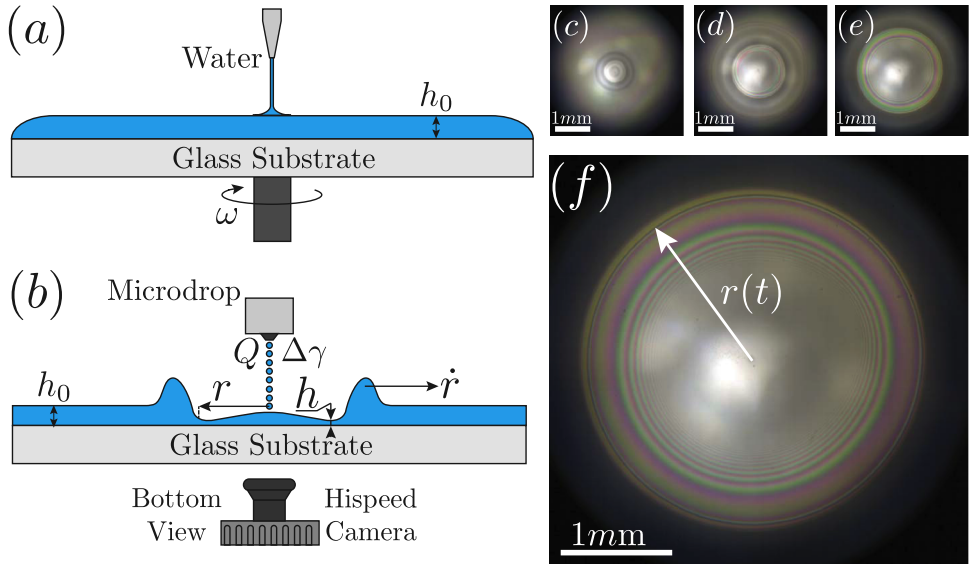

FIG. 1. (a) Sketch of the spin coater setup, depositing a uniform film of water of thickness h_0. (b) Sketch of the radial spreading dynamics viewed as cross-section. After placing the substrate on the inverted microscope, a color high-speed camera is used to record the process. A microdrop nozzle shoots droplets ($d \sim 50$ μm) with controlled frequency of an IPA-water mixture on the water layer. The flux Q of IPA-water induces a surface tension difference $\Delta\gamma$. (c–f) Bottom view of the typical experiment image from the inverted microscope at times $t = 5$ ms, $t = 37$ ms, $t = 97$ ms, $t = 157$ ms. The experimental conditions are $h_0 = 14$ μs, $Q = 157$ nl/s, $1\%IPA(Vol.)$. The interferometry patterns are the result of a small thickness in the region behind the outward moving front.

the supporting film can be deep or thin. Recently, the Marangoni flow of soluble surfactants on a deep pool was suggested as a tool to efficiently measure surfactant properties.[26] Most similar to our present study is the axisymmetric spreading on thin films, which for spreading of a fixed amount of surfactant and from a continuous source, respectively, leads to $r \sim t^{1/4}$[19,23,25,27,28,32–35] and $r \sim t^{1/2}$.[31] In all cases, the spreading was observed to be faster on films of larger thickness.[36–38]

In this paper, we experimentally determine the scaling law for the Marangoni spreading due to a continuous flux of miscible liquid (isopropyl alcohol (IPA)-water mixture) on a water film. It is found that for all conditions, $r \sim t^{1/2}$, while accurate control over the liquid composition and deposition allows us to quantify how the prefactor of this law depends on the experimental parameters. Interestingly, this gives a different picture than expected in comparison to the case of surfactant spreading. Based on our detailed measurements, we can derive a scaling theory that captures all observations. In Sec. II, we describe the experimental setup, the measurements, and the calibrations required to achieve well controlled quantitative experiments. In Sec. III, we present measurements of the radius of the opening hole as a function of time for different conditions. Here, we present the scaling arguments that describe the process as the dynamic balance between the Marangoni and viscous stresses. The paper ends with a Discussion in Sec. IV.

II. EXPERIMENTAL SETUP

We start by describing the experimental setup, measurement procedure, and necessary calibrations. Two steps were followed for each experiment. First, a water layer of uniform thickness is deposited on a hydrophilic substrate using a spin coater [Fig. 1(a)]. The thickness h_0 is varied from 8 to 70 μm, where h_0 is determined using a high-resolution spectrometer (Ocean optics HR4000). The substrate consists of a silica glass slide (71×71 mm), which is made hydrophilic using the cleaning procedure described in the Appendix. This cleaning step is critical to achieve reproducible results. Second, the substrate with the film is placed on the inverted microscope (Zeiss Axiovert 25), with a high speed color camera (Photron SA2) recording the bottom view [Fig. 1(b)]. A Marangoni

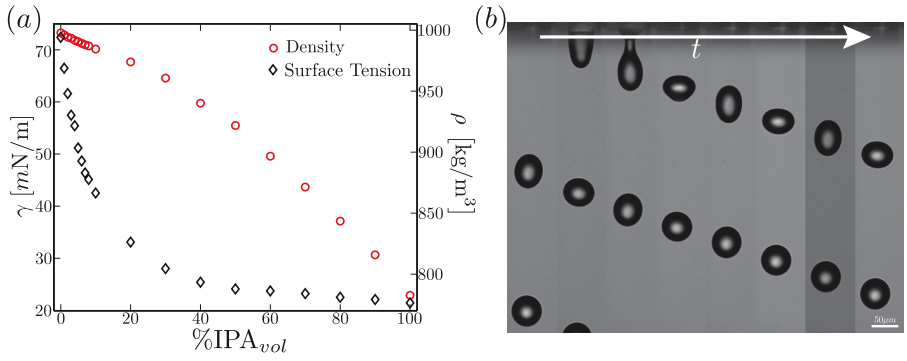

FIG. 2. (a) Calibration of the density (○, right vertical axis) and the surface tension (◇, left vertical axis) as a function of IPA concentration. (b) Visualization of the generation of microdrops, obtained using iLIF technique developed by Ref. 42. From these type of images, we could determine the range over which the monodisperse train of droplets was generated, and determine the corresponding flow rates Q. The horizontal scale bar corresponds to 50 μm.

flow is created by a continuous supply of micron-sized drops of an IPA-water mixture, deposited on top of the water film. The IPA-water mixture has a lower surface tension than water, giving rise to localized depression of surface tension and hence Marangoni forces. As seen in Figs. 1(c)-1(f), these forces induce a radially outward flow in the form of a circular traveling front, leaving behind a liquid layer much thinner than the initial thickness. The small drops that are deposited at the center of the images have negligible inertia, ensuring that this radial spreading is solely driven by Marangoni forces. While the growth of the circular front is reminiscent of the classical "dewetting hole" (dry circular patches on partially wetting surfaces Brochard-Wyart and de Gennes[39]), a key difference is that here the substrate is perfectly wetting and a macroscopic liquid film remains in the interior.

The goal of the experiment is to reveal the dynamics of the spreading radius, $r(t)$, as a function of the control parameters of the experiment. The spreading radius is defined as the backside of the rim, as shown in Fig. 1(b). Through image analysis, we measure the spreading radius in the recordings. The concentric rings in the inner region appear due to constructive light interference. Using the color interferometry technique reported by Ref. 40, the fringes provide a measurement of the film thickness in the thinnest region. We performed experiments by systematically varying the initial film thickness h_0, the flow rate of the IPA-water drops Q, as well as the composition of the IPA-water mixture. By changing the composition, we vary the surface tension and the density as has been calibrated in Fig. 2(a). The density and the surface tension were measured using a density-meter (DM A35 from Anton Paar) and the pendant drop method (tensiometer OCA15 Pro-Dataphysics). These calibrations show excellent agreement with Ref. 41, who previously measured surface tension and viscosity measurements of IPA-water mixtures. We vary the flow rate Q by varying the frequency at which the microdrops are deposited. The exact flow rate is calibrated using the imaging technique developed by van der Bos *et al.*[42] Figure 2(b) shows a typical image of the train of droplets that are generated. We measure the droplet size for each deposition frequency and compute the corresponding flow rate Q.

III. RESULTS AND SCALING LAWS

We start by considering a 1% (in volume) concentration IPA-water mixture that is deposited at a flow rate Q = 150.7 nl/s, onto films of varying initial thickness h_0. The results are presented in Fig. 3(a), showing the spreading radius as a function of time on a log-log plot. We observe that the radius scales as $r \sim t^{1/2}$. Below, we will show that this scaling law is very robust and observed for all experiments.

Quite unexpectedly, the data in Fig. 3(a) reveal that the radius $r(t)$ is completely independent of the initial thickness of the water layer. This is in marked contrast with the classical view on spreading due to localized deposition of surfactants,[20,36–38,43] for which scaling laws are usually built upon

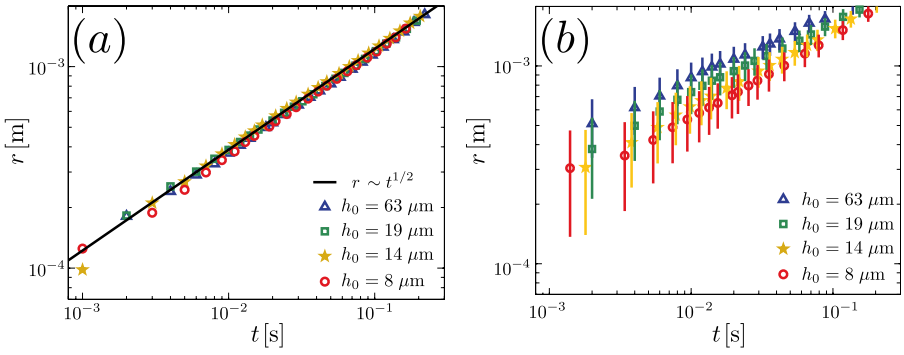

FIG. 3. (a) Spreading radius $r(t)$ as a function of time for different thicknesses of the water layer film h_0. The symbols (△), (□), (★), and (○), respectively, correspond to initial water layer thickness $h_0 = 63\ \mu$m, $h_0 = 19\ \mu$m, $h_0 = 14\ \mu$m, and $h_0 = 8\ \mu$m, respectively. The liquid flow to the surface is $Q = 150.7$ nl/s and the isopropanol concentration is 1% which leads to a surface tension difference $\Delta\gamma = 5.56$ mN/m. The initial time is taken at the instant of contact observed in the recordings. The dynamics of the spreading radius is found to be independent of the initial water layer thickness h_0. Each curve is the average of three experiments under the same conditions. (b) Radius of the "outer rim" $r_{\text{out}}(t)$, as defined in Fig. 4. Despite limited accuracy, one observes that the outer front develops more rapidly over water layers of larger thickness.

the initial thickness h_0. However, we were able to observe an influence of h_0 on the dynamics *ahead* of the rim. Figure 4 shows two snapshots under identical conditions, both taken at t = 15 ms, but with a different thickness. One very clearly observes the inside of the front (denoted as inner rim), which we have used before to measure $r(t)$. The horizontal yellow lines show that this inner rim has the same radius in both Figs. 4(a) and 4(b), confirming their dynamics to be independent of h_0. However, the width of the rim is clearly different in both cases: the outer rim has evolved over a larger distance on the image on the left (larger thickness) than on the right (smaller thickness). The position of the outer rim is much more difficult to resolve here, but for completeness, we have reported the dynamics of the outer radius $r_{\text{out}}(t)$ in Fig. 3(b). The front advances more rapidly on thicker water layer. Given the difficulty to accurately determine the outer front, we will from now on focus on the dynamics of the inner radius. The central goal is to find out what determines its dynamics, if we cannot use h_0 as a characteristic length scale.

Next, we consider the influence of the flux Q on the inner rim dynamics, $r(t)$, while keeping the IPA concentration constant at 1%. The variation in the flux Q spans nearly three orders of

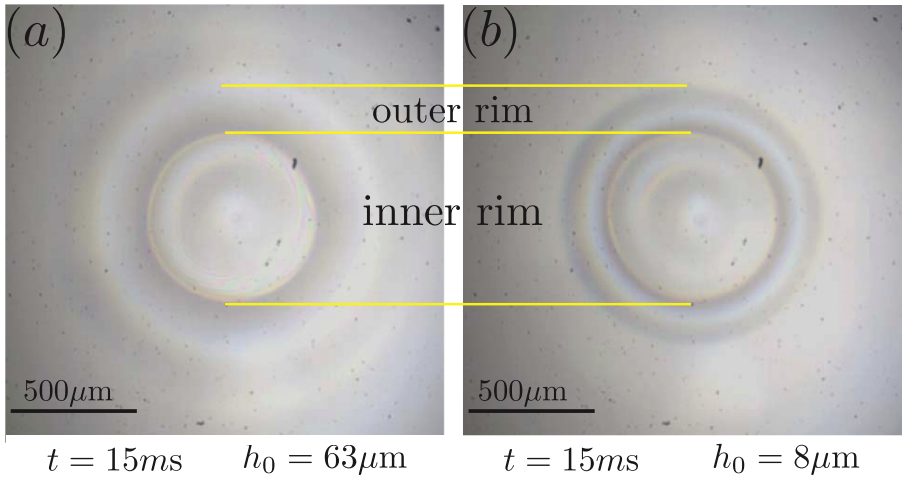

FIG. 4. Comparing two experiments of different initial thickness: $h_0 = 63\mu$m (a) and $h_0 = 8\ \mu$m (b). The dynamics of the "inner rim" (lower yellow lines) is identical in both cases. By contrast, the "outer rim" (upper yellow line) advances more rapidly for larger h_0.

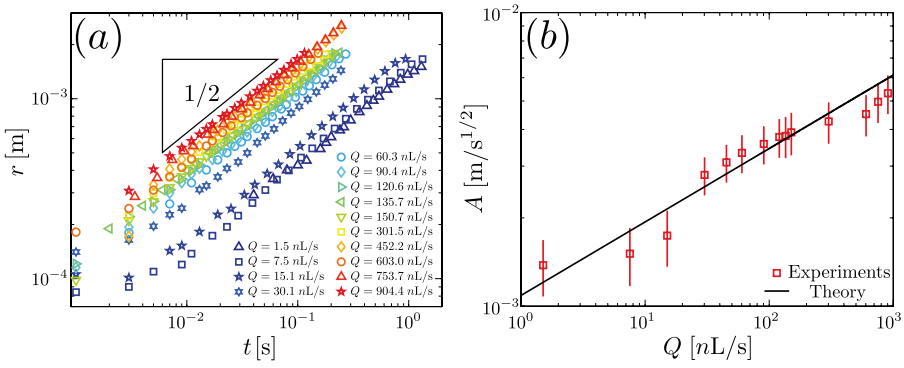

FIG. 5. (a) Measurement of the spreading radius as a function of time for different rates of IPA-water supply (Q = 1.5 nl/s–904 nl/s). The spreading dynamics follows $r(t) = At^{1/2}$, where the prefactor A increases with Q. (*b*) The fitted values of A as a function of the flow rate Q. The solid line corresponds to the predicted scaling law $A \sim Q^{1/4}$, with a prefactor 0.7 (best fit). The initial thickness in these experiments is $h_0 = 14\ \mu$m.

magnitude from 1.5 nl/s to 904.4 nl/s. The initial thickness in these experiments is kept constant at $h_0 = 14\ \mu$m. In Fig. 5(a), we show the radius as a function of time for different Q. This result confirms that the spreading law $r \sim t^{1/2}$ is very robust, for all rates at which IPA is supplied. However, we do observe a clear influence of Q on the dynamics: increasing the flow rates leads to a faster Marangoni flow. To quantify this result, we fitted the curves in Fig. 5(a) by

$$r = A\, t^{1/2}, \tag{1}$$

and determined the prefactor A as a function of Q. As shown in Fig. 5(b), the data are consistent with the power-law, $A \sim Q^n$. Fitting the value of the exponent, we obtain $n = 0.23 \pm 0.02$. Below, we argue that this corresponds to a scaling exponent $n = 1/4$, which is shown as the solid black line.

We now provide a scaling law to explain these observations. Contrary to the situation encountered for surfactants,[43] the scaling laws for the inside of the hole should not involve the thickness of the initial layer h_0. We start by considering the driving force generated by a Marangoni stress,

$$\tau_M = \frac{d\gamma}{dr} \sim \frac{\Delta\gamma}{r}, \tag{2}$$

where $\Delta\gamma$ is the surface tension difference between the two liquids. Such a Marangoni stress in the interface will induce a Couette-like profile inside the thin film, of typical radial velocity v_r. By scaling the stress as $1/r$, we assume that the surface tension difference spreads out over the entire radius of the inner circle (see also Ref. 26). Clearly, these type of arguments do not capture detailed spatial structure of the IPA-concentration profile, nor the dependence shown in Fig. 2(a)–yet they enable to capture the essential physics of the Marangoni-flow, as will become apparent below.

The Marangoni-stress τ_M is opposed by a viscous stress τ_η, which for thin film flows reads

$$\tau_\eta = \eta \frac{dv_r}{dz} \sim \eta \frac{\dot{r}}{h}, \tag{3}$$

where η is the viscosity and h is the characteristic thickness of the film. In the last step, we estimated the radial fluid velocity v_r by the velocity of the inside of the rim, $\dot{r} = dr/dt$. This is not obvious *a priori*, since, in general, the motion of the free surface profile need not be proportional to the fluid velocity. However, based on similarity assumptions that are common for this type of spreading problems,[43] we assume that the rim position $r(t)$ is the only relevant length scale for the *kinematics* of the radial flow. It then naturally follows that $v_r \sim \dot{r}$. Combining this with the *dynamic* condition, i.e., balancing the stresses $\tau_M \sim \tau_\eta$, we find

$$\frac{\Delta\gamma}{r} \sim \eta \frac{\dot{r}}{h}. \tag{4}$$

Crucially, we have seen that the initial thickness of the film h_0 is irrelevant for the dynamics. Hence, we assume that the characteristic thickness h appearing in Eq. (4) corresponds to the thin film at the interior of the circle, the thickness of which is an unknown dynamical variable as well.

Its value can be identified using mass conservation: we assume the volume of liquid at the interior of the rim mostly originates from the deposited volume. The first volume scales as $\pi r^2 h$, while the latter is simply Qt. This gives a global mass balance

$$Qt \sim r^2 h, \tag{5}$$

which after differentiation with respect to time gives the scaling law

$$Q \sim r h \dot{r}. \tag{6}$$

We later on justify that the typical height h can be considered constant over the course of the experiment. Equation (6) reflects that the incoming flow rate Q generates a liquid flux that scales like the rim velocity $\dot{r}$ multiplied by the area defined by the perimeter times liquid thickness, $2\pi r h$.

Combined with Eq. (4), we can eliminate h and obtain

$$Q \sim \frac{\eta}{\Delta\gamma}\, r^2\, \dot{r}^2, \tag{7}$$

or equivalently,

$$r \sim \left(\frac{Q\,\Delta\gamma}{\eta}\right)^{1/4} t^{1/2} \quad \Longrightarrow \quad A = k\left(\frac{Q\,\Delta\gamma}{\eta}\right)^{1/4}. \tag{8}$$

Here, we introduced k as a numerical prefactor that we expect to be of order unity.

These scaling arguments indeed explain the two key experimental observations: $r \sim t^{1/2}$ and $A \sim Q^{1/4}$. In addition, Eq. (8) gives a prediction for A in terms of the known parameters $\Delta\gamma = 5.56$ mN/m, and $\eta = 0.95$ mPa s. We use the dataset in Fig. 3(b) to determine the numerical prefactor k. The black solid line (best fit) indeed corresponds to a value of order unity, namely, $k = 0.7$.

To further test the validity of the scaling theory, we perform a set of experiments changing the isopropanol concentration in the IPA-water mixture from 0.05% to 23%. This changes both the surface tension and the viscosity of the IPA-water mixture, which in practice means that we have to recalibrate the settings of the microdrop for a given frequency and isopropanol concentration. Therefore, by changing the IPA concentration, we vary Q, η, and $\Delta\gamma$ at the same time. Yet, all values have been calibrated independently, allowing for a quantitative comparison to the theory. In Fig. 6(a), we present the results for the different IPA-water mixtures, corresponding to a large range of surface tension differences, from $\Delta\gamma = 0.3$ mN/m to 40 mN/m. Once more, we find $r \sim t^{1/2}$

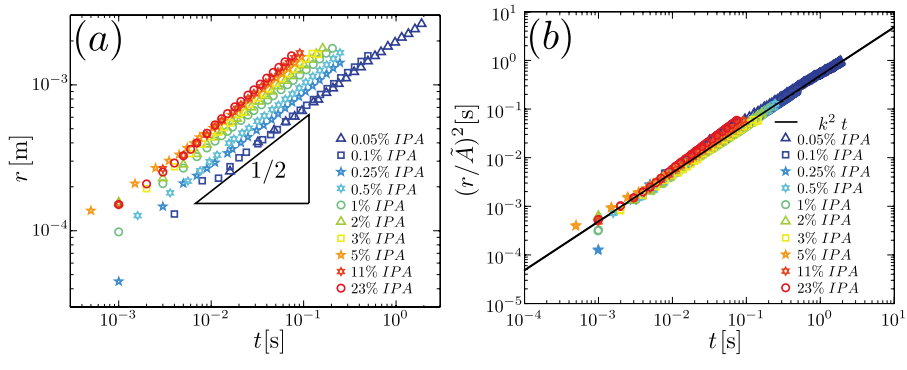

FIG. 6. (a) Measurement of the spreading radius r as a function of time for different experiments using different isopropanol concentrations. The initial time is taken at the instant of contact observed in the recordings. The isopropanol concentrations were varied from 0.05% to 23% which lead to surface tension differences from $\Delta\gamma = 0.3$ mN/m to 40.61 mN/m. (b) Collapsed curve for the various isopropanol concentrations. The curves were normalized using $A = (Q\Delta\gamma/\eta)^{1/4}$. The initial thickness in these experiments is $h_0 = 14\ \mu$m.

and we can directly test the prediction for A. To this end, we try to collapse the data by plotting $(r/\tilde{A})^2$, where $\tilde{A} = (Q\,\Delta\gamma/\eta)^{1/4}$ should account for the parametric dependence. Indeed, the data nicely collapse as shown in Fig. 6(b), without adjustable parameter. The solid line corresponds to the theory with $k = 0.7$, as obtained from our previous fit. We conclude that the scaling theory very well describes our experimental observations.

Finally, one can solve the thickness of the thin film h by combining Eqs. (4) and (8). As anticipated, the various scaling laws are such that the thickness is independent of time

$$h \sim \left(\frac{\eta\, Q}{\Delta\gamma}\right)^{1/2}, \tag{9}$$

and which is expressed in terms of known quantities. For the experiment in Figs. 1(c)-1(f), these are $\Delta\gamma = 5.56$ mN/m, $Q = 150.7$ nl/s, and $\eta = 0.95$ mPa s, such that $h \sim 5.1$ μm. This estimate gives the characteristic thickness of the region inside of the circular region. Owing to the fringes observed just behind the moving front [see, e.g., Fig. 1(f)], we can locally determine the film thickness using the interferometry technique developed by Ref. 40. Indeed, we obtain a thickness that during the course of the experiment is approximately constant, within a range of ±250 nm, and that is determined by $h \sim 1.4$ μm. It is a bit smaller than the prediction by the scaling law (9), though still of comparable magnitude. In addition, we note that the central region has a larger thickness, as the fringes are no longer visible.

IV. DISCUSSION AND CONCLUSIONS

In this paper, we analyzed Marangoni spreading due to the injection of an IPA-water mixture on a water film. Using a microdrop generator, we were able to supply the IPA in a very localized area and at controlled flow rates, allowing for a detailed quantitative study of the spreading. The experimentally observed dynamics was explained through a balance between Marangoni and viscous stresses, and we proposed scaling laws that were verified in detail by a data-collapse.

A key ingredient of the dynamics is that the surface tension gradient is spread out over the entire radius of the opening hole, i.e., $d\gamma/dr \sim \Delta\gamma/r$. This reduces the Marangoni driving force as the radius grows, which is why the spreading velocity decreases during the course of the experiment. This slowing down is markedly different from the "delayed coalescence," observed when two sessile drops of miscible liquids come into contact.[6–10] Rather than coalescing, the drop of the larger surface tension was found to pull the other drop at constant velocity over the substrate. Such a constant velocity suggests that the surface tension gradient remains constant and localized where the two fluids meet, at least during the initial stages of the experiment.[9]

The decrease in gradient observed in the present paper is much more reminiscent of the surfactant spreading,[24,25,28] though some remarkable differences do appear. In particular, we have found that the initial thickness of the film does not affect the dynamics of the central zone. Most closely resembling the present work is the case where surfactants are continuously supplied in a way that their total mass increases linearly in time. However, it is usually assumed that the liquid volume is unchanged, i.e., the surfactant is supplied by a flow rate in units of area per time.[43] In our experiment the IPA is provided in a volumetric rate, hence increasing the volume of liquid in the film—as expressed in Eq. (6). This subtle difference gives a different input in the scaling laws, and explains why for the present case the influence of the initial thickness drops out of the analysis. It emphasizes the key importance of the flow geometry on Marangoni flows. Finally, we remark that the dynamics ahead of the opening hole *is* affected by the initial film thickness. Such differences between upstream and downstream dynamics are generic for surfactant spreading, though intriguingly, the difference was not predicted for the case of continuous supply of surfactant (area per unit time).[43]

A priori, it is not obvious to what extent the IPA-water drops can be considered as a surfactant. For this, one would need to know the detailed spatial distribution of the IPA concentration in water, both in the radial direction and across the depth of the liquid film. It is clear that the influence of diffusion needs to be considered for this.[44,45] The duration of a typical experiment is about 0.1 s and the diffusion constant for IPA in water is $D \sim 10^{-9}$ m^2/s, which leads to a diffusion length of

$L = 10\ \mu$m. This length is indeed totally negligible with respect to the radial scale, but only a bit larger than the characteristic thickness of the film. Hence, a lubrication approach for which the IPA is assumed to average quickly over the depth is not perfectly justified, but also the IPA does not remain perfectly at the interface. Similar to recent work on surfactants,[46] it would be interesting to further explore experimental possibilities to obtain more detailed information on the IPA distribution and the implications for the resulting Marangoni flow. We emphasize, however, that the results obtained here by experiment and scaling analysis capture the essential physical mechanisms.

ACKNOWLEDGMENTS

We are grateful to I. Cantat, B. Dollet, S. Karpitschka, D. Lohse, and H. Riegler for many interesting discussions. We also thank M.-J. van der Meulen and E. Sandoval-Nava for their help in the microdrop device calibration. This work is sponsored by Lam Research, STW and NWO by VIDI Grant No. 11304.

APPENDIX: CALIBRATIONS

We use the following cleaning procedure to give hydrophilic properties to a silica glass slide (71 mm × 71 mm). A precleaned glass slide is rinsed with pure water (resistivity $\mathcal{R} = 18.2\ \mathrm{M\Omega}$), wiped with an aqueous solution of a soap (1%aq Hellmanex III), rinsed with pure water, then with isopropanol, and dried with nitrogen. Afterwards, the substrate is placed inside a plasma cleaner (Harrick Plasma PDC-002) for 3 min at 1.8 millibars. The hydrophilicity of this process is tested measuring the contact angle of a sessile drop of water.

To create the uniform water layer on the film, we fix the substrate on a spin coater with a vacuum pump. This is shown in Fig. 1(a). Then, we continuously supply water to the substrate while spinning during 10 s. Afterwards, the water supply stops and the rotation continues for 10 s more. The resulting thickness is measured as a function of the spin rate (from 200 rpm to 600 rpm). The thickness is measured using a High-Resolution spectrometer (Ocean optics HR4000), similar to Refs. 47 and 48.

We use a microdrop dispenser system (Microdrop Technologies MD-E-3000) to deposit a continuous supply of an IPA-water mixture on top of the water layer. The microdrop dispenser produces a continuous train of drops at frequencies varying from 1 Hz to 6000 Hz. For each IPA-water mixture, we calibrate the settings of the microdrop. This calibration consists of finding microdrop settings that produce a monodisperse train of drops and measure the typical drop diameter, using the technique presented by Ref. 42, see Fig. 2(b). This measurement is performed synchronizing a camera with the piezo pulse and a laser. The camera takes a picture at each cycle with a successive controlled delay. Different pictures at different moments of time allow to reconstruct the evolution of the stream of drops leaving the microdrop nozzle. The series of pictures are used to measure the drop diameter. The exact flow rate is calibrated by measuring the droplet size for each frequency. In order to achieve mono disperse size drops, we do trial and error tests under different conditions.

[1] A. E. Hosoi and J. W. M. Bush, "Evaporative instabilities in climbing films," J. Fluid Mech. **442**, 217–239 (2001).
[2] A. F. M. Leenaars, J. A. M. Huethorst, and J. J. Van Oekel, "Marangoni drying: A new extremely clean drying process," Langmuir **6**(11), 1701–1703 (1990).
[3] J. Marra and J. A. M. Huethorst, "Physical principles of Marangoni drying," Langmuir **7**(11), 2748–2755 (1991).
[4] O. K. Matar and R. V. Craster, "Models for Marangoni drying," Phys. Fluids **13**(7), 1869–1883 (2001).
[5] S. B. G. M. O'Brien, "On Marangoni drying: Nonlinear kinematic waves in a thin film," J. Fluid Mech. **254**, 649–670 (1993).
[6] H. Riegler and P. Lazar, "Delayed coalescence behavior of droplets with completely miscible liquids," Langmuir **24**(13), 6395–6398 (2008).
[7] S. Karpitschka and H. Riegler, "Quantitative experimental study on the transition between fast and delayed coalescence of sessile droplets with different but completely miscible liquids," Langmuir **26**(14), 11823–11829 (2010).
[8] R. Borcia and M. Bestehorn, "Partial coalescence of sessile drops with different miscible liquids," Langmuir **29**(14), 4426–4429 (2013).
[9] S. Karpitschka and H. Riegler, "Noncoalescence of sessile drops from different but miscible liquids: Hydrodynamic analysis of the twin drop contour as a self-stabilizing traveling wave," Phys. Rev. Lett. **109**(6), 066103 (2012).
[10] S. Karpitschka and H. Riegler, "Sharp transition between coalescence and non-coalescence of sessile drops," J. Fluid Mech. **743**, R1 (2014).

[11] W. D. Ristenpart, P. M. McCalla, R. V. Roy, and H. A. Stone, "Coalescence of spreading droplets on a wettable substrate," Phys. Rev. Lett. **97**(6), 064501 (2006).
[12] R. D. Narhe, D. A. Beysens, and Y. Pomeau, "Dynamic drying in the early-stage coalescence of droplets sitting on a plate," Europhys. Lett. **81**(4), 46002 (2008).
[13] M. W. Lee, D. K. Kang, S. S. Yoon, and A. L. Yarin, "Coalescence of two drops on partially wettable substrates," Langmuir **81**(8), 3791–3798 (2012).
[14] J. F. Hernández-Sánchez, L. A. Lubbers, A. Eddi, and J. H. Snoeijer, "Symmetric and asymmetric coalescence of drops on a substrate," Phys. Rev. Lett. **109**(18), 184502 (2012).
[15] T. Bohr, V. Putkaradze, and S. Watanabe, "Averaging theory for the structure of hydraulic jumps and separation in laminar free-surface flows," Phys. Rev. Lett. **79**, 1038–1041 (1997).
[16] D. Bonn, A. Andersen, and T. Bohr, "Hydraulic jumps in a channel," J. Fluid Mech. **618**, 71–87 (2009).
[17] A. Duchesne, L. Lebon, and L. Limat, "Constant Froude number in a circular hydraulic jump and its implication on the jump radius selection," Europhys. Lett. **107**(5), 54002 (2014).
[18] M. S. Borgas and J. B. Grotberg, "Monolayer flow on a thin film," J. Fluid Mech. **193**, 151–170 (1988).
[19] D. P. Gaver and J. B. Grotberg, "The dynamics of a localized surfactant on a thin film," J. Fluid Mech. **213**, 127–148 (1990).
[20] O. E. Jensen, "Self-similar, surfactant-driven flows," Phys. Fluids **6**(3), 1084–1094 (1994).
[21] O. K. Matar and S. M. Troian, "Spreading of a surfactant monolayer on a thin liquid film: Onset and evolution of digitated structures," Chaos **9**(1), 141–153 (1999).
[22] M. R. E. Warner, R. V. Craster, and O. K. Matar, "Fingering phenomena associated with insoluble surfactant spreading on thin liquid films," J. Fluid Mech. **510**, 169–200 (2004).
[23] M. R. E. Warner, R. V. Craster, and O. K. Matar, "Fingering phenomena created by a soluble surfactant deposition on a thin liquid film," Phys. Fluids **16**(13), 2933–2951 (2004).
[24] D. W. Fallest, A. M. Lichtenberger, C. J. Fox, and K. E. Daniels, "Fluorescent visualization of a spreading surfactant," New J. Phys. **12**(7), 073029 (2010).
[25] E. R. Peterson and M. Shearer, "Radial spreading of a surfactant on a thin liquid film," Appl. Math. Res. Express **2011**(1), 1–22.
[26] M. Roché, Z. Li, I. M. Griffiths, S. Le Roux, I. Cantat, A. Saint-Jalmes, and H. A. Stone, "Marangoni flow of soluble amphiphiles," Phys. Rev. Lett. **112**(20), 208302 (2014).
[27] J. B. Grotberg and D. P. Gaver III, "A synopsis of surfactant spreading research," J. Colloid Interface Sci. **178**(1), 377–378 (1996).
[28] A. Hamraoui, M. Cachile, C. Poulard, and A. M. Cazabat, "Fingering phenomena during spreading of surfactant solutions," Colloids Surf., A **250**(1), 215–221 (2004).
[29] J. Ahmad and R. S. Hansen, "A simple quantitative treatment of the spreading of monolayers on thin liquid films," J. Colloid Interface Sci. **38**(3), 601–604 (1972).
[30] S. M. Troian, E. Herbolzheimer, and S. A. Safran, "Model for the fingering instability of spreading surfactant drops," Phys. Rev. Lett. **65**(3), 333 (1990).
[31] O. E. Jensen and J. B. Grotberg, "The spreading of heat or soluble surfactant along a thin liquid film," Phys. Fluids A **5**(1), 58–68 (1993).
[32] M. R. E. Warner, R. V. Craster, and O. K. Matar, "Linear stability analysis of an insoluble surfactant monolayer spreading on a thin liquid film," Phys. Fluids **9**, 3645–3657 (1997).
[33] M. Cachile, A. M. Cazabat, S. Bardon, M. P. Valignat, and F. Vandenbrouck, "Spontaneous spreading of surfactant solutions on hydrophilic surfaces," Colloids Surf., A **159**(1), 47–56 (1999).
[34] A. D. Dussaud, O. K. Matar, and S. M. Troian, "Spreading characteristics of an insoluble surfactant film on a thin liquid layer: Comparison between theory and experiment," J. Fluid Mech. **544**, 23–51 (2005).
[35] O. K. Matar and R. V. Craster, "Dynamics of surfactant-assisted spreading," Soft Matter **5**(20), 3801–3809 (2009).
[36] D. K. Sinz, M. Hanyak, and A. A. Darhuber, "Immiscible surfactant droplets on thin liquid films: Spreading dynamics, subphase expulsion and oscillatory instabilities," J. Colloid Interface Sci. **364**(2), 519–529 (2011).
[37] D. K. Sinz, M. Hanyak, J. C. Zeegers, and A. A. Darhuber, "Insoluble surfactant spreading along thin liquid films confined by chemical surface patterns," Phys. Chem. Chem. Phys. **13**(20), 9768–9777 (2011).
[38] M. Hanyak, D. K. Sinz, and A. A. Darhuber, "Soluble surfactant spreading on spatially confined thin liquid films," Soft Matter **8**(29), 7660–7671 (2012).
[39] F. Brochard-Wyart and P. G. de Gennes, "Dynamics of partial wetting," Adv. Colloid Interface Sci. **39**, 1–11 (1992).
[40] R. C. A. van der Veen, T. Tran, D. Lohse, and C. Sun, "Direct measurements of air layer profiles under impacting droplets using high-speed color interferometry," Phys. Rev. E **85**(2), 026315 (2012).
[41] T. T. Ngo, T. L. Yu, and H.-L. Lin, "Influence of the composition of isopropyl alcohol/water mixture solvents in catalyst ink solutions on proton exchange membrane fuel cell performance," J. Power Sources **225**, 293–303 (2013).
[42] A. van der Bos, A. Zijlstra, E. Gelderblom, and M. Versluis, "iLIF: Illumination by laser-induced fluorescence for single flash imaging on a nanoseconds timescale," Exp. Fluids **51**(5), 1283–1289 (2011).
[43] O. E. Jensen and J. B. Grotberg, "Insoluble surfactant spreading on a thin viscous film: Shock evolution and film rupture," J. Fluid Mech. **240**, 259–289 (1992).
[44] R. Borcia, S. Menzel, M. Bestehorn, S. Karpitschka, and H. Riegler, "Delayed coalescence of droplets with miscible liquids: Lubrication and phase field theories," Eur. Phys. J. E **34**(3), 1–9 (2011).
[45] O. E. Jensen, "The spreading of insoluble surfactant at the free surface of a deep fluid layer," J. Fluid Mech. **293**, 349–378 (1995).
[46] E. R. Swanson, S. L. Strickland, M. Shearer, and K. E. Daniels, "Surfactant spreading on a thin liquid film: Reconciling models and experiments," J. Eng. Math. (published online 2014).
[47] J. H. Snoeijer, J. Ziegler, B. Andreotti, M. Fermigier, and J. Eggers, "Thick films of viscous fluid coating a plate withdrawn from a liquid reservoir," Phys. Rev. Lett. **100**(24), 244502 (2008).
[48] J. Seiwert, C. Clanet, and D. Quéré, "Coating of a textured solid," J. Fluid Mech. **669**, 55–63 (2011).